Received: 28 December 2024 | Revised: 12 March 2025 | Accepted: 24 March 2025

DOI: 10.1002/pro.70121

RESEARCH ARTICLE

THE PROTEIN SOCIETY WILEY

The role of phospholipid saturation and composition in α-synuclein aggregation and toxicity: A dual in vitro and in vivo approach

Aidan P. Holman[1,2] | **Tianyi Dou**[2] | **Mikhail Matveyenka**[2] | **Kiryl Zhaliazka**[2] | **Anjni Patel**[2] | **Avery Maalouf**[2] | **Ragd Elsaigh**[2] | **Dmitry Kurouski**[1,2,3]

[1]Interdisciplinary Faculty of Toxicology, Texas A&M University, College Station, Texas, USA

[2]Department of Biochemistry and Biophysics, Texas A&M University, College Station, Texas, USA

[3]Department of Biomedical Engineering, Texas A&M University, College Station, Texas, USA

Correspondence
Dmitry Kurouski, Interdisciplinary Faculty of Toxicology, Texas A&M University, College Station, Texas 77843, USA.
Email: dkurouski@tamu.edu

Funding information
National Institute of General Medical Sciences, Grant/Award Number: R35GM142869

Review Editor: Jean Baum

Abstract

Parkinson's disease is characterized by a progressive accumulation of α-synuclein (α-syn) aggregates in Lewy bodies, extracellular deposits found in the midbrain, hypothalamus, and thalamus. The rate of α-syn aggregation, as well as the secondary structure of α-syn oligomers and fibrils, can be uniquely altered by lipids. However, the role of saturation of fatty acids (FAs) in such lipids in the aggregation properties of α-syn remains unclear. In this study, we investigated the effect of saturation of FAs in phosphatidylcholine (PC) and cardiolipin (CL), as well as a mixture of these phospholipids on the rate of α-syn aggregation. We found that although saturation plays very little if any role in the rate of protein aggregation and morphology of α-syn aggregates, it determined the secondary structure of α-syn oligomers and fibrils. Furthermore, we found that aggregates formed in the presence of both saturated and unsaturated PC and CL, as well as mixtures of these phospholipids, exert significantly higher cell toxicity compared to the protein aggregates formed in the lipid-free environment. To extend these findings, we conducted in vivo studies using *C. elegans*, where we assessed the effect of lipid-modified α-syn aggregates on organismal survival and neurotoxicity. Our results suggest that the saturation of FAs in phospholipids present in the plasma and mitochondrial membranes can be a key determinant of the secondary structure and, consequently, the toxicity of α-syn oligomers and fibrils. These findings provide new insights into the role of lipids in Parkinson's disease pathogenesis and highlight potential targets for therapeutic intervention.

KEYWORDS
AFM-IR, alpha-synuclein, amyloids, lipids, oligomers

1 | INTRODUCTION

Parkinson's disease (PD) is the second-most common neurodegenerative disorder among senior people (Poewe et al., 2017). Clinical studies of PD revealed the presence of extracellular deposits known as Lewy bodies (LBs) in the midbrain, hypothalamus, and thalamus (Rambaran & Serpell, 2008; Wischik et al., 1985, 1988). Histological analysis of LBs revealed the presence of α-synuclein (α-syn) aggregates. Although the actual physiological function of α-syn remains unclear, a growing body of evidence demonstrates that α-syn is involved in the regulation of neurotransmitter release and synaptic vesicle trafficking (Sidhu et al., 2004). Under pathological conditions, α-syn aggregates form oligomers and fibrils, highly toxic species that impair the physiological functions of neurons in the brain (Yamada & Iwatsubo, 2018). Cryo-electron microscopy (cryo-EM) was capable of resolving the secondary structure of α-syn fibrils (Guerrero-Ferreira et al., 2018,

2020; Li et al., 2018). It was found that α-syn fibrils were composed of two β-sheet filaments held together by hydrogen bonding. This highly stable structure, known as a cross β-sheet, stretched microns in length in the direction perpendicular to the peptide strands (Chiti & Dobson, 2017; Cremades et al., 2012). It was also found that α-syn filaments could braid and intertwine forming higher-order supramolecular assemblies, such as proto-fibrils and fibrils (Guerrero-Ferreira et al., 2018; Heise et al., 2005; Li et al., 2018; Tuttle et al., 2016). At the same time, there is very little if anything known about α-syn oligomers (Chen et al., 2015). Primarily because their morphological heterogeneity limits the use of cryo-EM and solid-state NMR, classical tools of structural biology, for their structural characterization. It should be noted that Chen et al. were able to resolve the secondary structure of thermodynamically stable donut-like α-syn oligomers (Chen et al., 2015). It was found that these oligomers were dominated by β-sheet. Chen et al. also demonstrate that donut-like α-syn oligomers exerted significantly higher cell toxicity compared to both α-syn monomers and fibrils (Chen et al., 2015). Zhou and Kurouski found that α-syn oligomers formed at the early stages exhibited large diversity in protein secondary structures (Zhou & Kurouski, 2020a). Some of them were primarily composed of parallel β-sheet, whereas others had a mixture of anti-parallel β-sheet and α-helix. It was also found that the amount of anti-parallel β-sheet was gradually decreasing in the secondary structure of α-syn oligomers as they were propagating into fibrils.

Numerous pieces of experimental evidence show that lipids can uniquely alter the rates of protein aggregation (Frese et al., 2023; Jiang et al., 2013; Matveyenka, Rizevsky, Pellois, & Kurouski, 2023; Matveyenka, Zhaliazka, et al., 2022; O'Leary & Lee, 2019a; Pfefferkorn et al., 2012; Zhaliazka, Matveyenka, et al., 2023; Zhaliazka, Serada, et al., 2023). Galvagnion et al. found that in the presence of large unilamellar vesicles (LUVs) of phosphatidylserine (PS), α-syn aggregated much faster compared to the lipid-free environment (Galvagnion, 2017; Galvagnion et al., 2015a, 2016). These findings suggested that an increase in the concentration of PS in the outer layer of plasma membranes could facilitate the primary nucleation of α-syn in the brain. Recently reported results by Dou et al. demonstrated lipids not only changed the rate of protein aggregation but also uniquely altered the secondary structure of α-syn oligomers (Dou et al., 2021; Dou & Kurouski, 2022b; Galvagnion et al., 2015b). Specifically, α-syn oligomers grown in the presence of PS and phosphatidylcholine (PC) had drastically different secondary structures compared to α-syn oligomers formed in the lipid-free environment (Dou et al., 2021; Dou & Kurouski, 2022b; Galvagnion et al., 2015b). Similar conclusions were made by Matveyenka et al. about insulin and lysozyme fibrils formed in the presence of different phospho- and sphingolipids (Kotarek & Moss, 2010; Matveyenka, Rizevsky, & Kurouski, 2022a, 2022b, 2022c; O'Leary & Lee, 2019b; Pirc & Ulrih, 2015; Trostchansky et al., 2005). Furthermore, Matveyenka and co-workers found that saturation of fatty acids (FAs) in phospholipids could uniquely alter the rate of protein aggregation (Kotarek & Moss, 2010; Matveyenka, Rizevsky, & Kurouski, 2022a, 2022b, 2022c; O'Leary & Lee, 2019b; Pirc & Ulrih, 2015; Trostchansky et al., 2005). It was demonstrated that in the presence of unsaturated cardiolipin (CL) (u-CL), insulin aggregated much faster compared to CL with saturated FAs (s-CL). Matveyenka and co-workers also found that insulin fibrils formed in the presence of u-CL and s-CL had drastically different secondary structures and, as a result, exerted significantly different cell toxicity (Matveyenka, Rizevsky, & Kurouski, 2022c). Zhaliazka et al. demonstrated that CL and cholesterol could drastically alter the aggregation rates of amyloid $\beta_{1\text{-}42}$ ($A\beta_{1\text{-}42}$), a peptide that is expected to be the underlying molecular cause of Alzheimer's disease (Zhaliazka, Matveyenka, et al., 2023). It was also found that $A\beta_{1\text{-}42}$ aggregates formed in the presence of CL and cholesterol had drastically different secondary structures compared to $A\beta_{1\text{-}42}$ aggregates grown in the lipid-free environment (Zhaliazka, Matveyenka, et al., 2023). This precise analysis of the secondary structure of amyloid aggregates was performed by atomic force microscopy infrared (AFM-IR) spectroscopy, an emerging analytical technique that could be used to probe the secondary structure of individual amyloid oligomers and fibrils (Dou et al., 2022; Dou & Kurouski, 2022b; Kurouski et al., 2020; Ruggeri et al., 2015, 2020).

In this study, we utilized AFM-IR to investigate the secondary structure of α-syn aggregates formed in the presence of lipids that constitute a substantial fraction of the mitochondrial membrane. Specifically, we analyzed α-syn oligomers and fibrils formed in the presence of anionic unsaturated (u) and saturated (s) CL, as well as zwitterionic u-PC and s-PC. CL is a unique mitochondria phospholipid that constitutes around 20% of the inner mitochondrial membrane (Paradies et al., 2019). Under physiological conditions, CL primarily possesses unsaturated FAs. Upon mitochondrial stress, CL is exposed to the outer mitochondrial membrane where it can be oxidized by cytochrome C (Dudek, 2017). This results in the saturation of FAs in CL (Dudek, 2017). Both u- and s-PCs constitute around a third of all lipids in the plasma and organelle membrane of neurons (Choi et al., 2018). Therefore, it becomes critically important to understand the role of these lipids in α-syn aggregation. To further understand the effect of charge and saturation of phospholipids on α-syn aggregation, we also mixed u- and s-PC and CL in 20:80 (CL:PC) and 50:50 (CL:PC) ratios. These ratios of u- and s-phospholipids are important to determine whether the dominance of unsaturated anionic

(u-CL) or zwitterionic (u-PC) has a stronger effect on α-syn aggregation. Cellular toxicity assays were conducted on each of these conditions. In addition to the in vitro structural and toxicity analyses, we performed in vivo studies using *C. elegans* models to assess how lipid-modified α-syn aggregates influence organismal survival and neuronal toxicity. We anticipate that our findings provide valuable insights into the role of lipids in modulating the aggregation and toxicity of α-syn and in suggesting potential therapeutic targets for PD.

2 | RESULTS

2.1 | Kinetics of α-syn aggregation in the presence of individual phospholipids and lipid mixtures

We first performed kinetic measurements of α-syn aggregation in the presence of LUVs composed of individuals- and u-CL and PC, as well as PC/CL mixtures using the thioflavin T (Th-T) assay, Figure 1. Our results showed that the presence of s- and u-CL and PC LUVs did not alter the rate of protein aggregation. Specifically, we observed very similar, if not identical, t_{lag} and $t_{1/2}$ for α-syn and α-syn:s-CL, α-syn:u-CL, α-syn:s-PC, and α-syn:u-PC. These results demonstrated that phospholipids, as well as saturation of FAs in CL and PC, had very little, if any, effect on the rate of α-syn aggregation.

Similar conclusions could be made about α-syn aggregation in the presence of LUVs composed of both u- and s- PC and CL mixed at 50:50 and 80:20 molar ratios. We found that α-syn exhibited similar t_{lag} in the presence of all analyzed PC/CL mixtures. Our results also showed that only the s-PC:u-CL (50:50) mixture slightly decelerated the rate ($t_{1/2}$) of α-syn aggregation. However, the rate of α-syn aggregation in the presence of other lipid mixtures was identical to the rate of α-syn aggregation in the lipid-free environment. Finally, we found that the t_{growth} of all analyzed samples except α-syn:u-CL was the same. Only α-syn:u-CL fibrils grew faster than protein aggregates in all other samples. These results demonstrated that saturation of FAs of PC and CL in PC/CL mixtures had very little, if any, effect on α-syn aggregation.

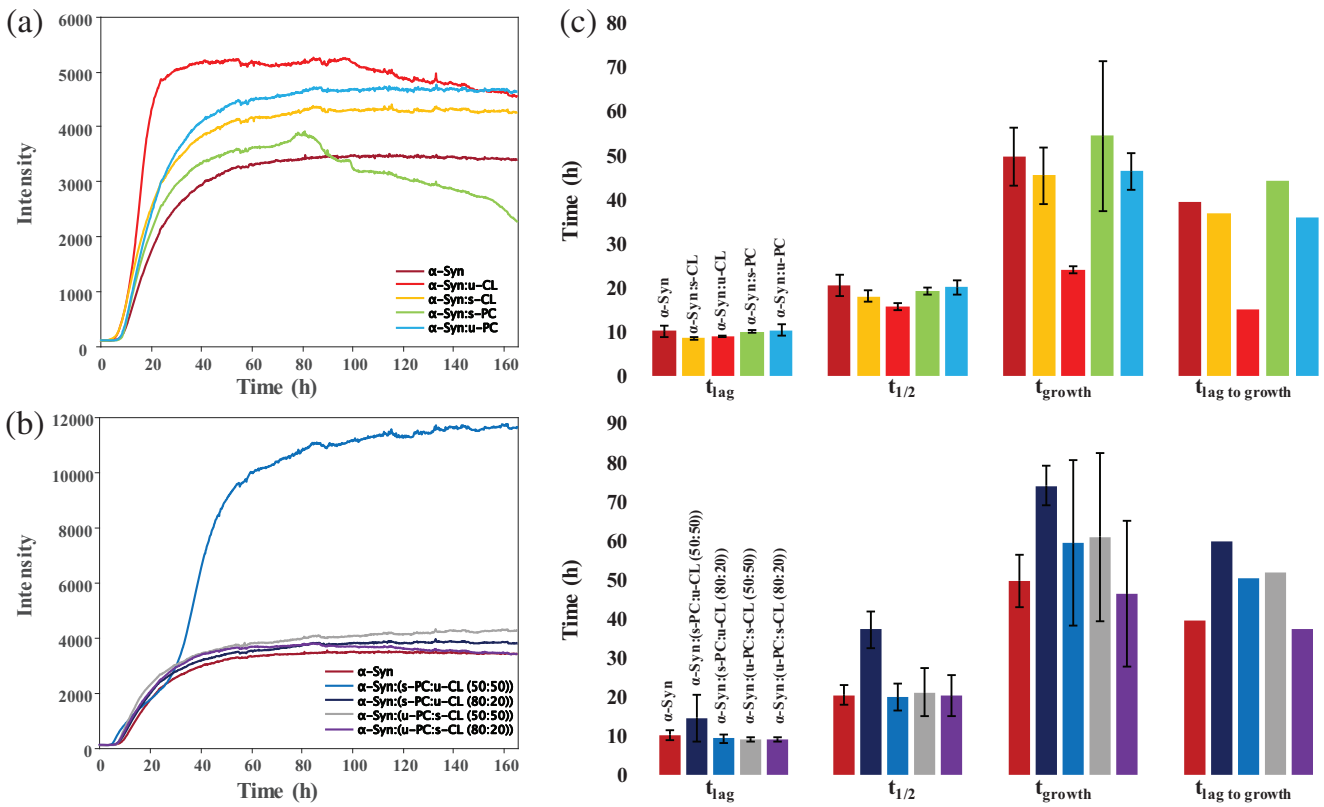

FIGURE 1 Kinetics of α-syn aggregation in the presence of s- and u-CL and PC (a) and PC/CL mixtures (b). A histogram (c) that summarizes the lag phase (t_{lag}, 10% of the maximum Th-T intensity), $t_{1/2}$ (50% of the maximum Th-T intensity), t_{growth} (90% of the maximum Th-T intensity), and growth–lag time (t_{growth}/t_{lag}) of α-syn aggregation in the presence of LUVs composed of individual phospholipids and lipid mixtures.

Expanding on this, we performed morphological and structural analysis of protein aggregates formed at the lag (12 h), growth (36 h), and plateau (60 h) of α-syn aggregation.

2.2 | Morphological characterization of α-syn aggregates formed in the presence of lipids and lipid mixtures

At the lag phase (12 h), in the presence of both s-CL and u-CL, α-syn formed only small oligomers, Figure 2. Morphologically similar oligomers were formed by α-syn in the presence of s- and u-PC, as well as in the presence of PC/CL mixtures. These oligomers had 5–7 nm in height. We also found similar protein species at the growth phase (36 h) of α-syn aggregation in the presence of individual lipids, as well as in the presence of PC/CL mixtures, Figure 2. However, long fibril species were observed in α-syn:u-CL in addition to the discussed above oligomers. We also found similar fibrillar species in α-syn:(s-PC:u-CL (50:50)) and α-syn:(u-PC:s-CL (50:50)). Finally, we found lipid-like clusters in α-syn:(s-PC:u-CL (80:20)) that were surrounded by small oligomers. This observation suggested that s-PC:u-CL (80:20) LUVs could template α-syn aggregation. All analyzed protein samples taken at the plateau (60 h) of α-syn aggregation possessed long flat fibrillar species, Figure 2. We also observed very few if any oligomers in these samples, which indicates that nearly all oligomers propagated into fibrils. It should be noted that α-syn fibrils formed in the presence of s- and u-PC and CL exhibited similar morphologies. We also observed morphologically similar fibrils formed in the presence of different lipid mixtures except for α-syn:(sPC:u-CL (50:50)), which had substantially thicker fibrils. These results showed that LUVs of individual lipids and lipid mixtures with saturated and unsaturated FAs had very little if any effect on the morphology of protein aggregates formed in their presence.

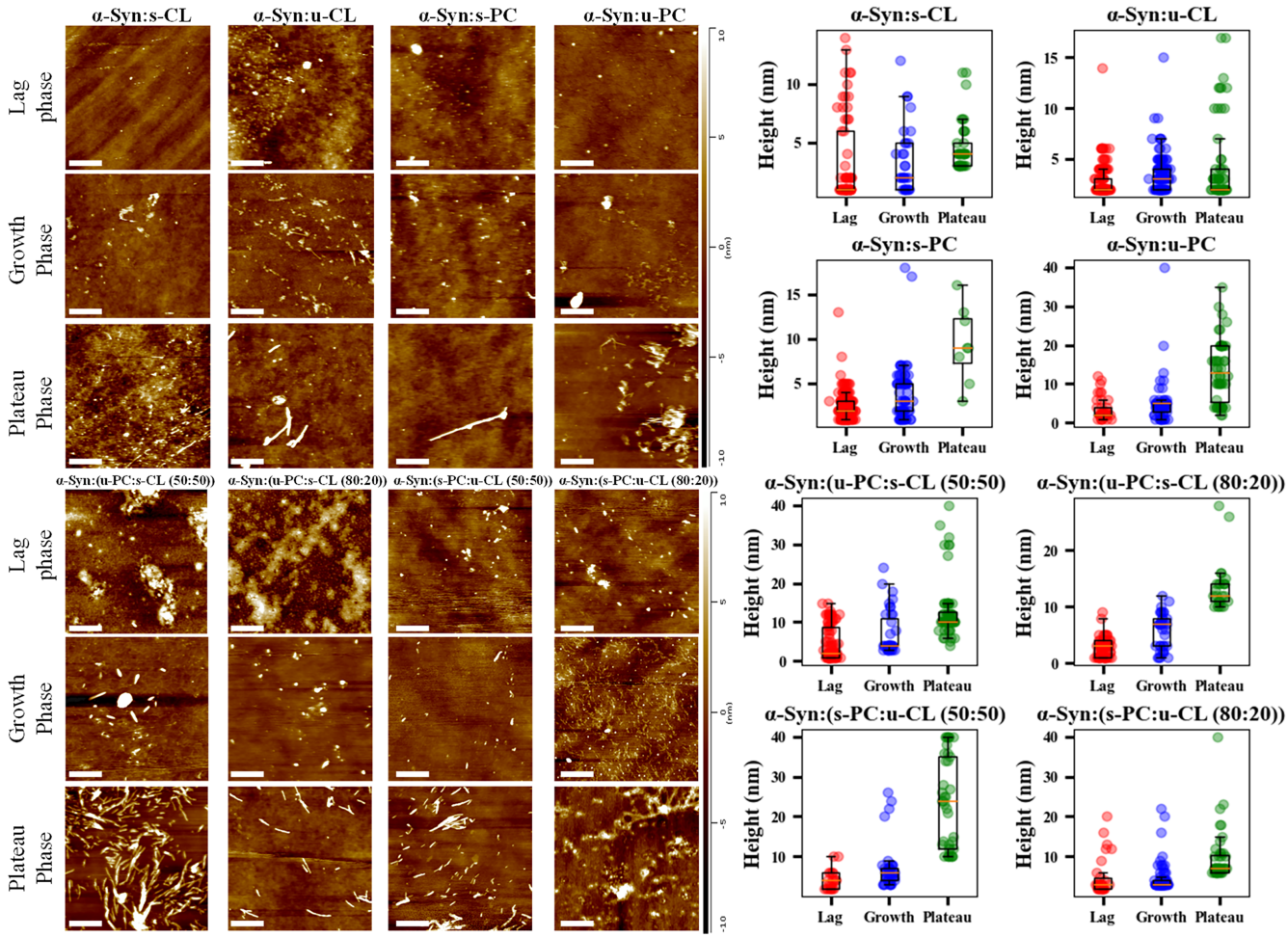

FIGURE 2 AFM images (left) and height profiles (right) of α-syn aggregates formed in the presence of s- and u-CL and PC, as well as in the presence of PC/CL mixtures at the lag, growth, and plateau of protein aggregation. The scale bars of all AFM images are 1 μm.

2.3 | Structural characterization of α-syn aggregates formed in the presence of lipids and lipid mixtures

We used AFM-IR to characterize the protein secondary structure of both oligomers and fibrils formed at the different stages of protein aggregation. In AFM-IR, the sample is illuminated by pulsed tunable IR light with the metalized scanning probe positioned precisely at the object of interest (Centrone, 2015; Chae et al., 2015; Dazzi et al., 2012; Dazzi & Prater, 2017; Katzenmeyer et al., 2014). The light causes thermal expansions in the sample that are recorded by the probe and converted into the IR spectrum (Ramer et al., 2017, 2018; Ruggeri, Benedetti, et al., 2018; Ruggeri, Charmet, et al., 2018). A growing body of evidence demonstrates that AFM-IR can be used to probe the secondary structure of individual proteins, as well as resolve the structural organization of amyloid oligomers, fibrils, polymers, and viruses (Banerjee & Ghosh, 2021; Ramer et al., 2018; Zhaliazka & Kurouski, 2022, 2023).

The acquired AFM-IR spectra exhibited an amide I band, which could be used to interpret the secondary structure of protein species. The amide I band at 1614–1624 cm^{-1} indicates the predominance of parallel β-sheet, whereas the shift of the amide I to 1640–1655 cm^{-1} is evidence of random coil and α-helical secondary structure. Finally, protein specimens with anti-parallel β-sheet exhibit amide I at 1694 cm^{-1}. We found substantial differences in the secondary structure of α-syn oligomers formed in the presence of u- and s-PC and CL at the lag-phase of the protein aggregation. Specifically, α-syn:u-PC and α-syn:u-CL oligomers were dominated by the random coil and α-helical secondary structures, whereas α-syn:s-PC and α-syn:s-CL oligomers, on the opposite, primarily possessed parallel β-sheet, Figure 3. It should be noted that, unlike α-syn:s-PC aggregates, α-syn:s-CL oligomers contained a substantial amount of anti-parallel β-sheet secondary structure. These results demonstrated that lipids uniquely altered the secondary structure of α-syn oligomers formed in the presence of LUVs. Furthermore, the secondary structure of such oligomers was determined by the saturation of FAs in these phospholipids.

The same conclusion could be made about α-syn:u- and α-syn:s-PC and CL aggregates observed at the growth phase of the protein aggregation. Specifically, we found that the secondary structure of both α-syn:s-CL, α-syn:s-, and α-syn:u-PC aggregates was dominated by parallel and anti-parallel β-sheet, whereas α-syn:u-CL oligomers had primarily random coil and α-helical secondary structure, Figure 3. Finally, AFM-IR analysis revealed that the secondary structure of mature fibrils of α-syn:u- and α-syn:s-PC and CL was dominated by parallel β-sheet with some amount of random coil, α-helical, and anti-parallel β-sheet secondary structure. Nevertheless, small changes in the position of the amide I band point to some difference in the secondary structure of α-syn:u- and α-syn:s-PC and CL fibrils. These results demonstrate that lipids uniquely altered the secondary structure of α-syn fibrils. Our findings also demonstrated that not only the charge of the lipid polar head but also the saturation of the FAs plays an important role in the determination of the secondary structure of α-syn aggregates formed in the presence of phospholipids.

We also performed AFM-IR imaging of α-syn oligomers formed in the presence of u- and s-PC and CL oligomers and fibrils at the lag, growth, and plateau stages of protein aggregation, Figures 4 and S1. AFM-IR imaging revealed that a vast majority of protein aggregates observed in each sample were structurally similar, if not identical. This observation suggested that lipids templated α-syn aggregation. We also found that nearly all aggregates collected at different time points were dominated by the parallel β-sheet secondary structure compared to the random coil and α-helical conformations, Figure 4. Most of the aggregates collected at the lag stage exhibited slightly higher anti-parallel β-sheet secondary structure than the random coil and α-helical conformations, Figure S2. These findings are consistent with the previously reported results by Dou et al.

Next, we utilized AFM-IR to probe the secondary structure of α-syn oligomers formed in the presence of lipid mixtures. We observed drastic differences in the secondary structure of α-syn oligomers formed in the presence of PC/CL mixtures at the lag phase. Specifically, we found that the secondary structure of α-syn:(s-PC:u-CL (80:20)) was dominated by parallel β-sheet, whereas α-syn:(s-PC:u-CL (50:50)) and α-syn:(u-PC:s-CL (50:50)) had parallel and anti-parallel β-sheet secondary structure. Finally, we found that the secondary structure of α-syn:(u-PC:s-CL (50:50)) oligomers formed at the growth phase of protein aggregation was dominated by random coil, α-helical, and anti-parallel β-sheet secondary structure.

AFM-IR revealed high similarities in the secondary structure of α-syn oligomers formed at the growth phase of protein aggregation in the presence of lipid mixtures. All observed aggregates possessed parallel and anti-parallel β-sheet, as well as some random coil and α-helical structures. One can expect that α-syn:(s-PC:u-CL (50:50)) had the lowest amount of random coil and α-helix, whereas α-syn:(s-PC:u-CL (80:20)), on the opposite, possessed the highest amount of this protein secondary structure. Finally, AFM-IR analysis of mature fibrils formed at the plateau of α-syn aggregation demonstrates that all aggregates have substantial amounts of parallel and anti-parallel β-sheet. AFM-IR imaging of α-syn aggregates formed in the presence of PC/CL

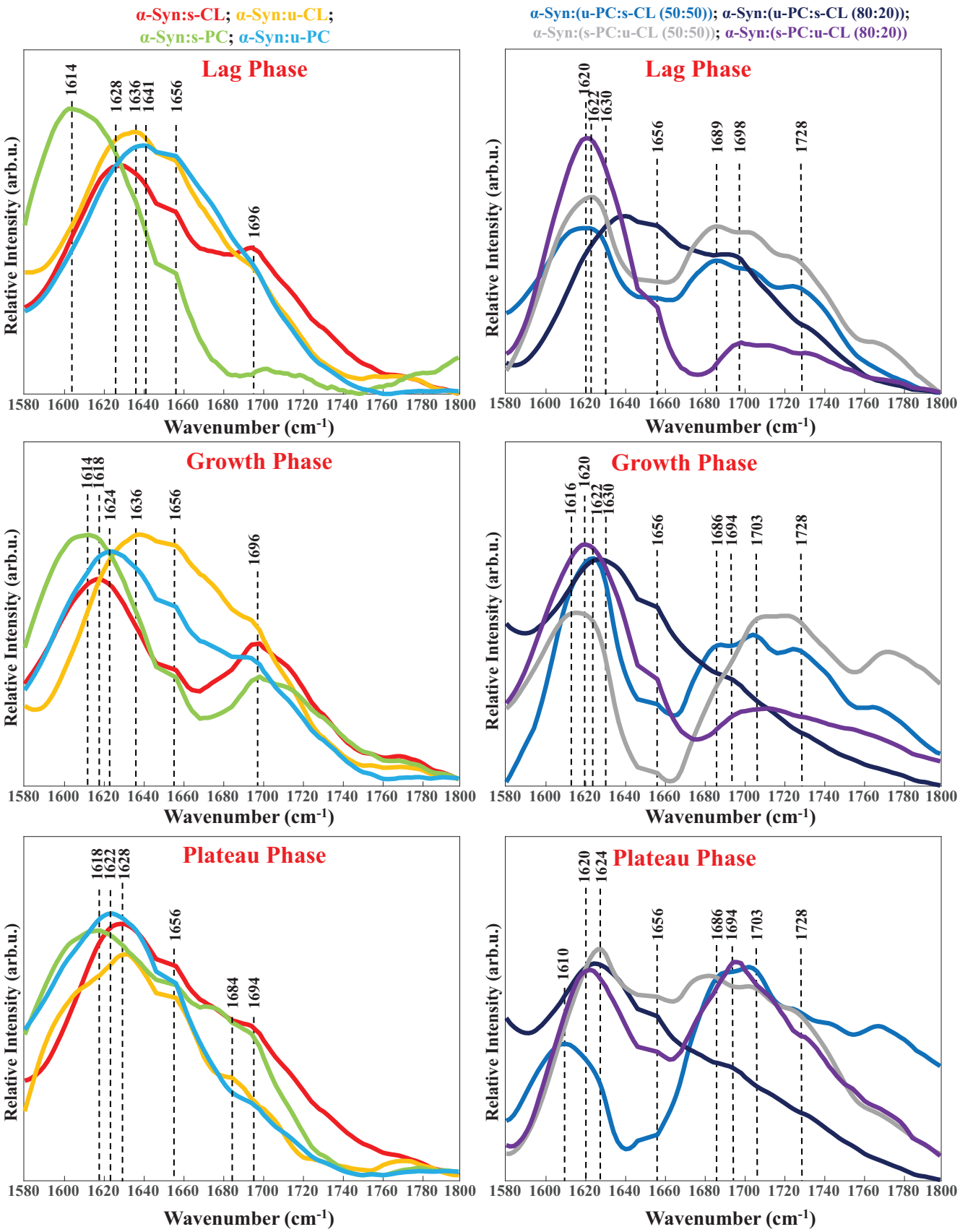

FIGURE 3 Averaged AFM-IR spectra acquired from α-syn aggregates formed in the presence of s- and u-CL and PC, as well as in the presence of PC/CL mixtures at the lag, growth, and plateau stages of protein aggregation.

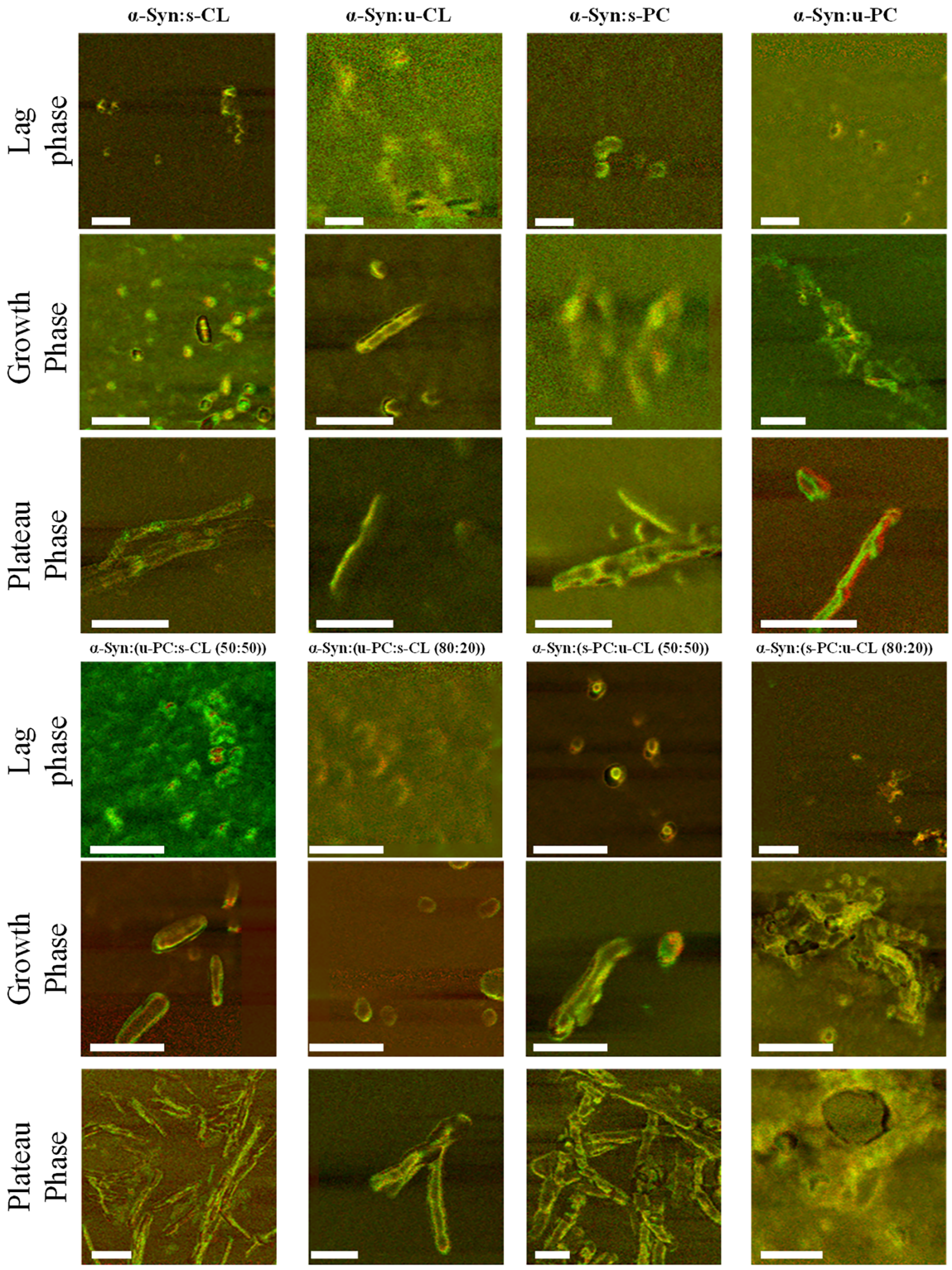

FIGURE 4 Overlapped IR chemical maps of α-syn aggregates grown in the presence of s- and u-CL and PC, as well as in the presence of PC/CL mixtures at lag, growth, and plateau phase. The maps were acquired at 1655 cm^{-1} (red), which represents the distribution of random coil and α-helix, and 1624 cm^{-1} (green), which corresponds to parallel β-sheet. The scale bars for all the maps are 200 nm.

mixtures at the lag, growth, and plateau stages of the protein aggregation is shown in Figures 3, S1 and S2. Nano-IR imaging indicated that the majority of the aggregates present in each sample were structurally similar, if not identical. This observation confirmed the discussion above, suggesting that lipids present in the lipid mixtures templated protein aggregation. This conclusion is also supported by the observed vibration

at ~1730 cm^{-1} in the AFM-IR spectra acquired from α-syn oligomers and fibrils formed in the presence of PC/CL lipid mixtures. This vibrational band can be assigned to the carbonyl (C═O) vibration of phospholipids (Matveyenka, Rizevsky, Pellois, et al., 2023). Based on these results, we can conclude that lipids are present in the structure of α-syn oligomers and fibrils formed in their presence. These findings are consistent with the previously reported results by Dou and co-workers (Dou et al., 2020, 2023; Dou & Kurouski, 2022a).

Next, we fitted the amide I band to determine the evolution of the protein secondary structure that was taking place upon oligomer propagation into fibrils, Figures 5 and S3. We found a gradual increase in the amount of parallel β-sheet in both α-syn:u-CL and α-syn:u-PC with a gradual decrease in the amount of random coil and α-helical secondary structure, Figure 5. At the same time, α-syn:s-CL aggregates exhibited drastically different evolution of the protein secondary structure. Specifically, we observed no changes in the amount of parallel β-sheet in their aggregates formed at the lag, growth, and plateau stages. α-syn:s-PC aggregates exhibited a small decrease in the amount of parallel β-sheet, while a small increase in the amount of random coil and α-helical secondary structure was observed between the aggregates formed at the lag and plateau stages of α-syn aggregation. Based on these results, we could conclude that the saturation of FAs in phospholipids uniquely altered the evolution of protein secondary structure that was taking place in the propagation of α-syn oligomer into mature fibrils. It should be noted that in the absence of lipids, α-syn aggregation, similar to α-syn:u-CL and α-syn:u-PC, proceeded with a gradual increase in the amount of parallel β-sheet.

Similar to α-syn:u-PC, we observed a gradual increase in the amount of parallel β-sheet in α-syn:(u-PC:s-CL (80:20)), as well as a decrease in the amount of anti-parallel β-sheet as the aggregates transform from growth to plateau stages, Figure 5. These results demonstrate that u-PC is the determining factor of protein secondary structure evolution in such a bilipid environment. The same conclusion could be made about α-syn:(s-PC:u-CL (80:20)) if compared to α-syn:s-PC. Specifically, we observed a gradual decrease in the amount of parallel β-sheet in the aggregates formed at the lag, growth, and plateau stages. These findings suggest that s-PC is the determining factor of protein secondary structure evolution in such a bilipid environment. It should be noted that the determining role of both u- and s-PC is concentration-dependent. Specifically, we observed drastically different evolution of the protein secondary structure of α-syn if the concentration of both u- and s-PC was lowered to 50% relative to the concentration of CL. In both cases (α-syn:(s-PC:u-CL (50:50)) and α-syn:(u-PC:s-CL (50:50))), we observed first an

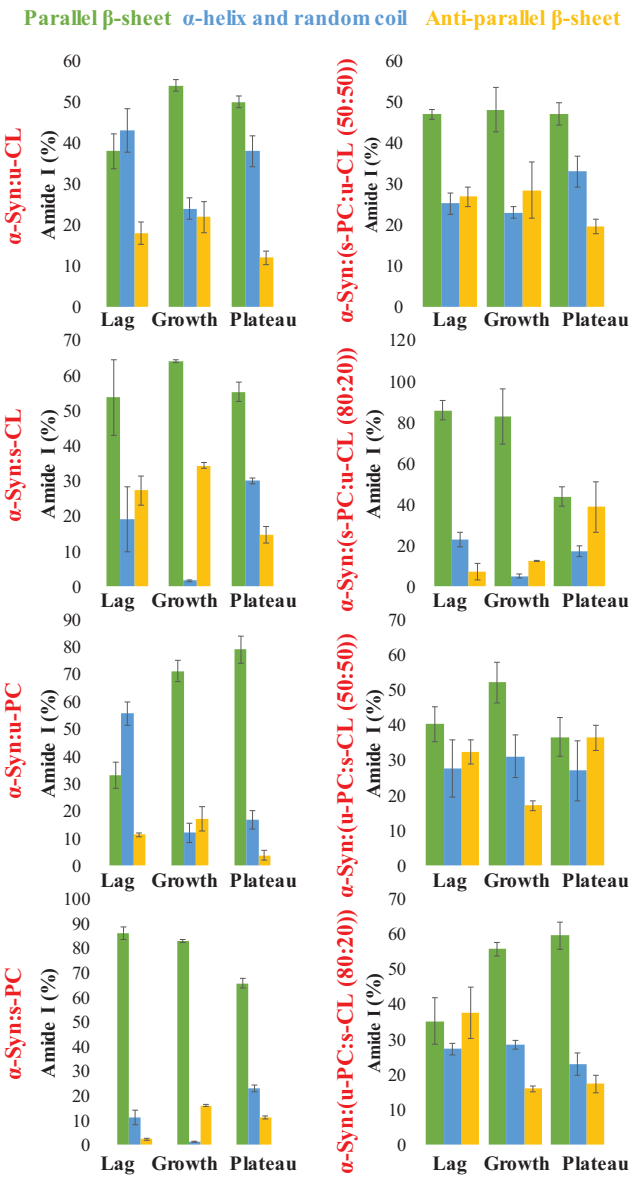

FIGURE 5 Bar graphs of protein secondary structure composition of α-syn aggregates formed in the presence of s- and u-CL and PC, as well as in the presence of PC/CL mixtures at the lag, growth, and plateau stages of protein aggregation, according to the fitting of amide I region of the AFM-IR spectra. Parallel β-sheet (peak at 1624 cm^{-1}) (green), α-helical and disordered structure (peak at 1655 cm^{-1}) (blue), and anti-parallel β-sheet (peak at 1694 cm^{-1}) (yellow).

increase and then a decrease in the amount of parallel β-sheet as the aggregates transformed from lag to growth and then from growth to plateau stages. Our results are in good agreement with these experimental findings reported by Frieg et al. that performed cryo-EM-based analysis of the secondary structure of α-syn fibrils formed in the presence of lipids (Frieg et al., 2022). It was found that lipids were incorporated in these protein aggregates. These researchers also found that lipid presence resulted in the alternative protofilament fold, which led to an unusual

arrangement of protofilaments and filled the central cavities of the fibrils. One can expect that the presence of α-helix and random coil on edges of mature α-syn fibrils could be explained by (i) parts of α-syn in the fibril that did not adopt β-sheet or (ii) as a result of side-templated (secondary) nucleation of mature fibrils. We also think that lipid present in such fibrils would promote folding of monomeric α-syn on the surface of fibrils into α-helix, which is detectable by AFM-IR.

2.4 | α-Syn aggregates formed in the presence of lipids exert significantly higher cell toxicity compared to the oligomers and fibrils formed in the lipid-free environment

α-Syn aggregates exert cell toxicity by enhancing ROS levels in cells while simultaneously impairing cell mitochondria. (Cascella et al., 2021; Chen et al., 2015; Dou et al., 2023). Therefore, we examined the extent to which α-syn aggregates formed at different stages of protein aggregation in the presence of individual lipids and lipid mixtures alter ROS levels in rat N27 dopaminergic cells. We also employed the JC-1 fluorescent assay to determine the extent to which such aggregates could damage mitochondrial membranes. Finally, we performed an LDH assay to reveal the relationship between the protein secondary structure of α-syn aggregates and their cytotoxicity, Figure 6. We found that α-syn oligomers formed in the presence of both u- and s-CL exerted significantly higher cell toxicity compared to α-syn oligomers formed in a lipid-free environment. We also found that the toxicity of α-syn:s-PC and α-syn:u-PC oligomers was much greater than the toxicity of α-syn:CL oligomers. Our results also showed that α-syn oligomers formed in the presence of PC/CL mixtures exerted even greater cell toxicity than the oligomers formed by α-syn in the presence of mono lipid LUVs. Based on these results, we can conclude that lipids enhanced the toxicity of α-syn oligomers. However, the opposite conclusion could be made about α-syn fibrils formed in the presence of lipids. Specifically, we found that α-syn:CL and α-syn:s-PC fibrils were less toxic to N27 rat neuronal cells than α-syn fibrils formed in a lipid-free environment. We did not observe statistically significant differences between the α-syn and α-syn:u-PC fibrils, as well as fibrils formed in the presence of PC/CL mixtures except α-syn:(s-PC:u-CL (50:50)), which appeared to be significantly more toxic than other fibril samples. Based on these results, we can conclude that lipids uniquely alter the toxicity of α-syn fibrils formed in their presence.

We found that ROS levels and the degree of mitochondrial impairment caused by α-syn and α-syn: lipid aggregates were similar to the discussed above LHD levels exerted by these specimens. Specifically, we found that α-syn:CL oligomers exert similar to α-syn oligomers levels of ROS and mitochondrial impairment to α-syn oligomers. However, all protein aggregates that were formed in the presence of PC engaged significantly greater ROS levels and mitochondrial impairment than α-syn oligomers formed in the lipid-free environment. These results demonstrated that α-syn:PC aggregates were highly toxic to N27 rat neuronal cells. These findings also demonstrated that the high toxicity of α-syn oligomers formed in the presence of lipid mixtures was, to a large extent, determined by PC rather than CL. Finally, our results showed that saturation of FAs in both PC and CL plays very little, if any, effect on the toxicity exerted by α-syn oligomers formed in the presence of such phospholipids.

At the same time, the saturation of FAs in PC plays an important role in the toxicity of α-syn fibrils. Specifically, we observed drastic differences in the levels of ROS stress exerted by α-syn:u- and α-syn:s-PC fibrils. Interestingly, the saturation of FAs in CL determined different levels of mitochondrial impairment caused by α-syn oligomers. Specifically, we found that α-syn:s-CL oligomers and fibrils exerted lower levels of mitochondrial damage compared to α-syn:u-CL. It should be noted that although the structural stability of fibrils in aqueous solvents is commonly accepted in the field of structural biology (Ramer et al., 2018), there is no clear understanding about the possible conformational changes that can take place in α-syn and α-syn:lipid oligomers after their exposition to the cell media. Using endosomal damage assays, our group previously demonstrated that such oligomers are rapidly endocytosed by neuronal cells (Ali et al., 2025; Matveyenka et al., 2024). This drastically minimizes their prolonged exposure to the cell media. Nevertheless, additional studies, which are beyond the scope of the current work, are required to fully understand the stability of α-syn and α-syn:lipid oligomers in cell media and, thus, establish a direct relationship between the secondary structure and toxicity of these protein aggregates.

2.5 | In vivo effects of phospholipid saturation and polar head groups on the lifespan of *C. elegans*

Our in vitro work served as the basis for our choices of phospholipids; in other words, we used 16-carbon chain phospholipids that are either fully saturated or unsaturated. These include unsaturated and saturated cardiolipin (U-CL and S-CL), phosphatidylcholine (U-PC and S-PC), and saturated phosphatidylglycerol (S-PG) and phosphatidylserine (S-PS). A lifespan assay (see Figure 7) of a transgenic *C. elegans*

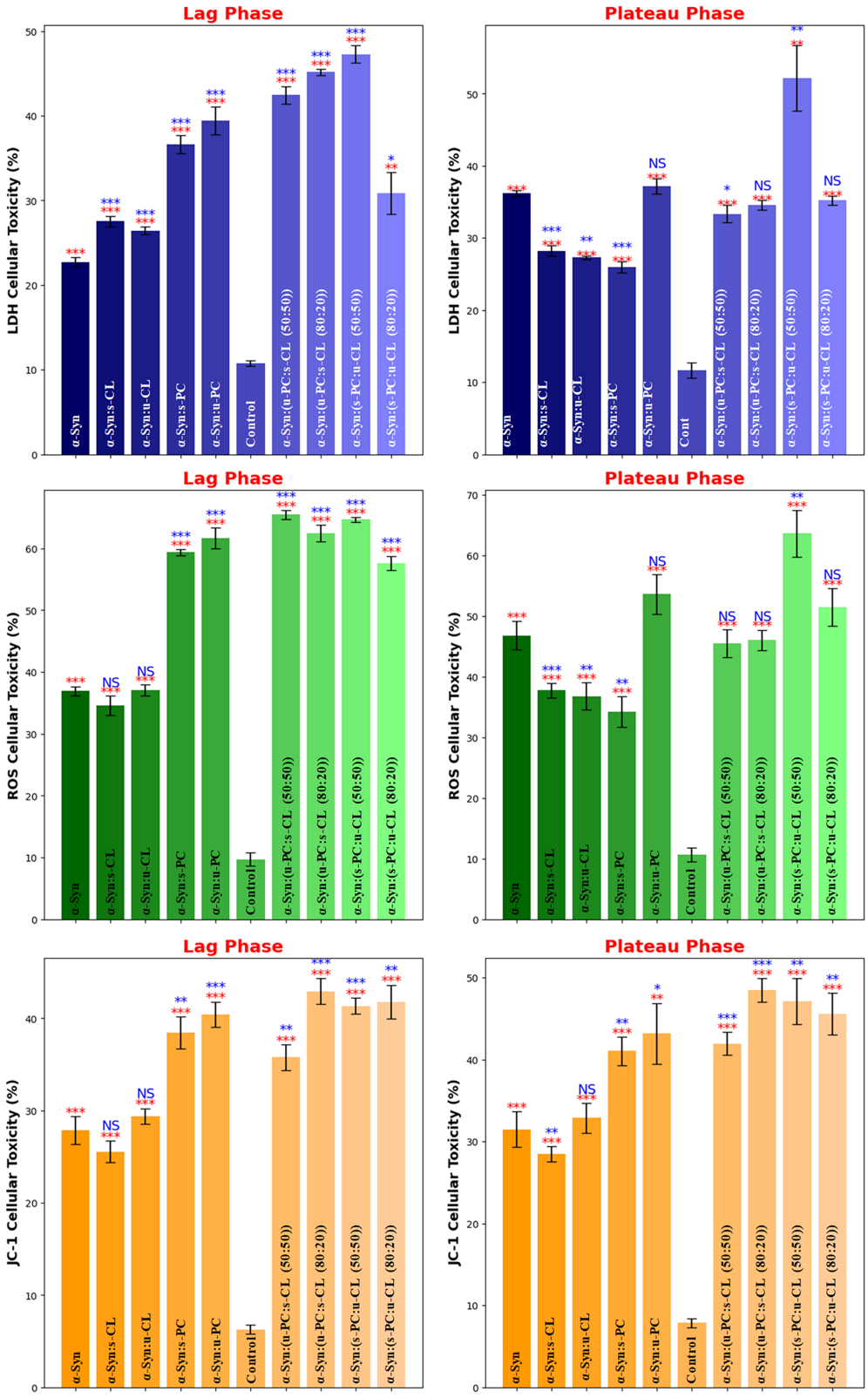

FIGURE 6 Bar graph of LDH (blue), ROS (green), and JC-1 (yellow) toxicity assays of α-syn aggregates grown in different lipid LUVs at the lag phase (left) and plateau stage (right) of protein aggregation. Blue asterisks (*) show the significance of the level of difference between α-syn in the lipid-free condition and α-syn aggregates grown in the presence of lipids. Red asterisks show the significance of the level of difference between α-syn aggregates and the control condition. NS is a nonsignificant difference, and $*p \leq 0.05$, $**p \leq 0.01$, and $***p \leq 0.001$.

(NL5901) that expresses α-syn fused to YFP in muscle cells was compared to the wild-type *C. elegans* strain, N2, to determine if the toxic effects elicited by the diets are species-specific or strain-specific. We found that in the N2 strain, many of the saturated phospholipid diets, such as S-PC, S-CL, and S-PG, did not show substantial changes in lifespan compared to the Control diet, with median lifespans ranging from 21 to 25 days, Table 1. However, the unsaturated diets, specifically U-PC and U-CL, led to a significant reduction in

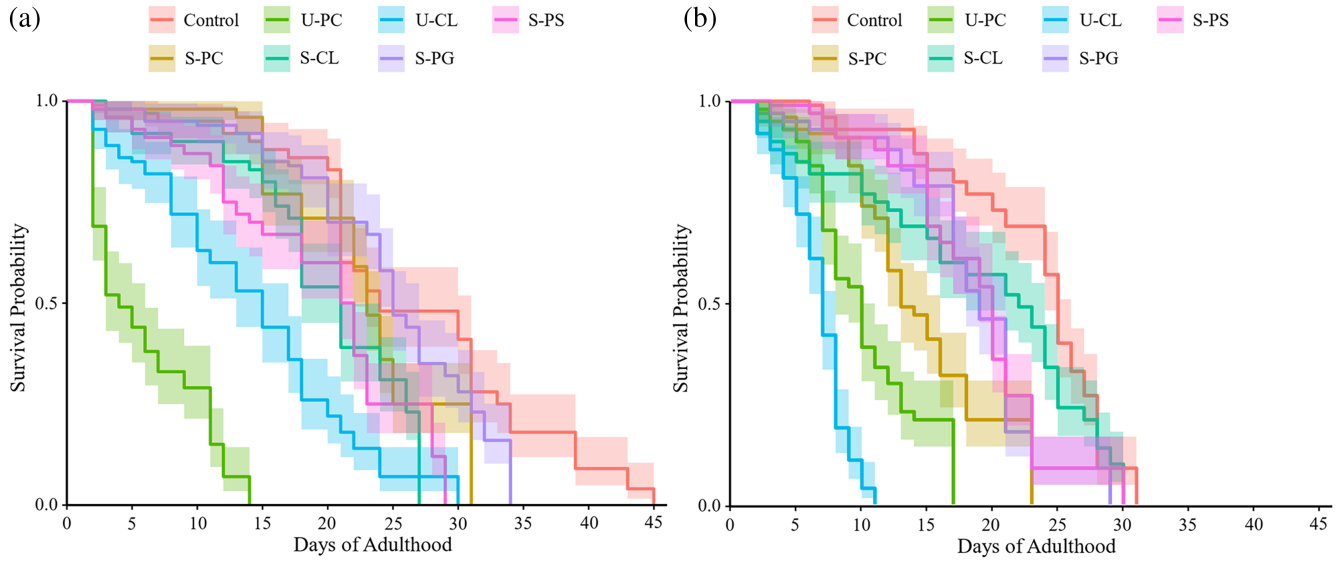

FIGURE 7 Kaplan–Meier survival curves for wild-type, N2, (a) and transgenic, NL5901, (b) *C. elegans* fed OP50 *E. coli* alone (Control) or in combination with 2.0% (w/v) U-PC, U-CL, S-PS, S-PC, S-CL, and S-PG.

TABLE 1 Median life expectancies for N2 and NL5901 *C. elegans* on various diets.

Strain	Diet	Median life expectancy (day)	Lower CI	Upper CI
N2	Control	24	22	31
	S-PC	23	23	24
	U-PC	4	3	6
	S-CL	21	18	21
	U-CL	15	13	17
	S-PG	25	24	27
	S-PS	21.5	21	22
NL5901	Control	25	24	26
	S-PC	13	12	16
	U-PC	10	8	10
	S-CL	22	18	24
	U-CL	7	7	8
	S-PG	19	18	21
	S-PS	20	19	20

lifespan, with U-PC resulting in a median lifespan of just 4 days and U-CL reducing it to 15 days. These findings are consistent across both strains, with the NL5901 strain showing even more pronounced effects from the unsaturated diets. For example, the U-PC and U-CL diets reduced the lifespan of NL5901 worms to 10 and 7 days, respectively. The S-CL diet was the only saturated phospholipid diet in the NL5901 strain that was similar to the Control diet, with a median lifespan of 22 days.

The Cox proportional hazards model results further emphasize the differing effects of diets on lifespan between strains, Table 2. The hazard ratios (HRs) and β-coefficients indicate that unsaturated diets, particularly U-PC and U-CL, are associated with significantly increased mortality in both strains. The HR for U-PC in the N2 strain is 4.265 ($p < 0.001$), and for NL5901, it is 5.244 ($p < 0.001$), suggesting a substantial increase in the risk of mortality compared to the Control diet. Similarly, U-CL shows a HR of 2.013 for N2 ($p < 0.05$) and 8.234 for NL5901 ($p < 0.001$), further supporting the toxicity of unsaturated diets. On the other hand, the saturated phospholipids, such as S-PS and S-PG, did not show significant increases in mortality risk, as indicated by their non-significant p-values and HRs close to 1. These results suggest that unsaturated phospholipids are more detrimental to lifespan, particularly in the transgenic NL5901 strain.

To compare the mortality risk between strains for each diet, Table 3 presents the results of a Wald test

TABLE 2 Coefficients, scores, and significance of diet effects on mortality in the Cox proportional hazards model of N2 and NL5901 *C. elegans* lifespan assays.

Strain	Diet	*β*-coefficient	Standard error	Hazard ratio	*Z*-score	*p*-value
N2	Control	–	–	1.0 (ref)	–	–
	S-CL	0.41	0.292	1.507	1.401	0.161
	S-PC	0.248	0.298	1.281	0.831	0.406
	S-PG	0.089	0.305	1.093	0.292	0.77
	S-PS	0.353	0.295	1.424	1.197	0.231
	U-CL	0.7	0.279	2.013	2.506	*
	U-PC	1.45	0.266	4.265	5.455	***
NL5901	Control	–	–	1.0 (ref)	–	–
	S-CL	0.376	0.493	1.456	0.763	0.446
	S-PC	1.262	0.442	3.531	2.852	**
	S-PG	0.741	0.469	2.097	1.579	0.114
	S-PS	0.652	0.476	1.919	1.37	0.171
	U-CL	2.108	0.43	8.234	4.903	***
	U-PC	1.657	0.435	5.244	3.812	***

*$p < 0.05$; **$p < 0.01$; ***$p < 0.001$.

TABLE 3 Determining whether the mortality risk of a diet is significant between strains using a Wald test [using log(HRs)].

Strain	Diet	Hazard ratio	Lower CI	Upper CI	*Z*-score	*p*-value
N2	S-CL	1.507	0.849	2.673	0.059	0.953
NL5901		1.456	0.554	3.826		
N2	S-PC	1.281	0.714	2.299	−1.9	0.057
NL5901		3.531	1.484	8.405		
N2	S-PG	1.093	0.601	1.988	−1.164	0.244
NL5901		2.097	0.837	5.258		
N2	S-PS	1.424	0.798	2.540	−0.533	0.594
NL5901		1.919	0.755	4.875		
N2	U-CL	2.013	1.165	3.479	−2.748	**
NL5901		8.234	3.545	19.127		
N2	U-PC	4.265	2.532	7.181	−0.406	0.685
NL5901		5.244	2.237	12.295		

*$p < 0.05$; **$p < 0.01$; ***$p < 0.001$.

on the log of hazard ratios. This analysis confirms that the differences in mortality risk between strains are significant for certain diets. For example, the HR for U-CL in the N2 strain is 2.013 ($p < 0.01$), while it is much higher in the NL5901 strain at 8.234 ($p < 0.001$), indicating a greater mortality risk for NL5901 worms. Likewise, the HR for U-PC is 4.265 for N2 and 5.244 for NL5901, with the latter being significant ($p < 0.001$), further demonstrating that the toxic effects of unsaturated diets are amplified in the NL5901 strain. The findings from the Cox model and Wald test suggest that diets significantly impact mortality, with unsaturated phospholipids consistently leading to greater toxicity, particularly in the transgenic NL5901 strain.

Overall, these results illustrate that phospholipid composition plays a crucial role in modulating the lifespan of *C. elegans*, with unsaturated phospholipids showing more pronounced toxic effects. Furthermore, the strain-specific differences observed in NL5901 suggest that the transgenic model may be more sensitive to these dietary changes, which may be linked to the expression of α-syn.

2.6 | In vivo effects of phospholipid saturation and polar head groups on the behavior of *C. elegans*

The swimming assay results for *C. elegans* strains N2 (Figure 8a) and NL5901 (Figure 8b) show the effects of various phospholipid diets on behavior at different time points (days 1, 5, 10, and 15). The data indicate that

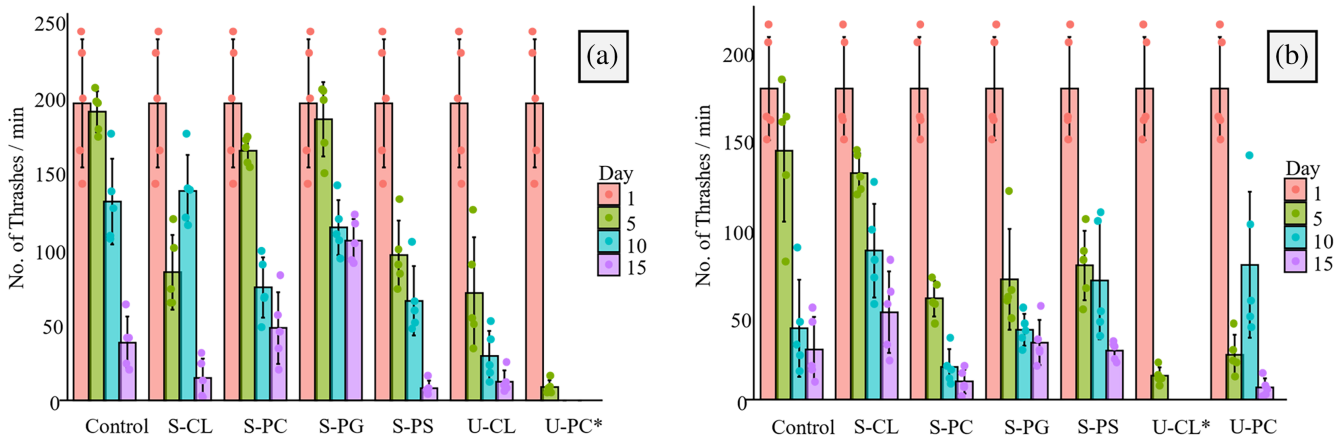

FIGURE 8 Swimming assay results for N2 (a) and NL5901 (b) *C. elegans* before (day 1) and after 5, 10, and 15 days of exposure to various diets.

diet and time both significantly influence the swimming behavior of the worms. For the N2 strain, comparisons to the control group revealed that by day 5, worms fed S-CL, S-PS, U-CL, and U-PC exhibited significantly lower ($p < 0.05$) swimming activity compared to the control diet. By day 10, only worms fed S-PS and U-CL continued to show reduced swimming behavior, while by day 15, no significant differences were observed across any of the diets. Additionally, when comparing the groups' behavior to day 1, worms fed S-CL, S-PC, S-PG, S-PS, U-CL, and U-PC exhibited reduced swimming at various time points, particularly at days 5 and 10. Interestingly, by day 15, only the control group showed a significant decrease in activity compared to day 1.

In contrast, the NL5901 strain exhibited a different pattern of results. By day 5, worms fed S-PC, S-PG, U-CL, and U-PC showed significantly lower swimming activity compared to the control group. However, by day 10 and day 15, no significant differences were observed between these diets and the control. When comparing the groups to day 1, worms on all diets except U-CL showed significant reductions in swimming at days 5, 10, and 15, with S-CL, S-PC, S-PG, S-PS, and U-PC consistently resulting in lower activity. U-CL, however, showed a decrease only at day 5. These findings suggest that while both strains are affected by phospholipid composition, the NL5901 strain exhibits more persistent reductions in swimming behavior, particularly with unsaturated diets, which may reflect strain-specific sensitivities or differences in the metabolic or genetic effects of these diets on the worms.

Overall, these results emphasize the complex, time-dependent effects of diet on worm behavior, with unsaturated phospholipids generally leading to quicker decreases in swimming activity compared to saturated diets. The limitations of the significantly toxic effects of these diets were noted in the absence of data at days 10 and 15 for the U-PC diet for N2 worms and the U-CL diet for NL5901 worms.

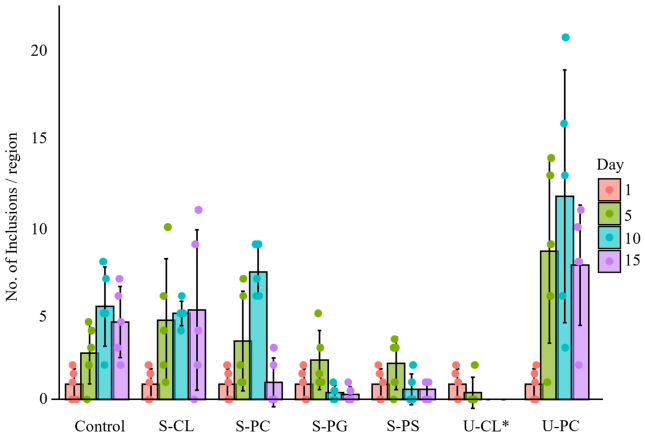

FIGURE 9 The total number of α-syn inclusions found in the head region (from anterior to the posterior pharynx) of NL5901 *C. elegans* before (day 1) and after 5, 10, and 15 days of exposure to various diets.

2.7 | In vivo effects of phospholipid saturation and polar head groups on large α-syn deposition in *C. elegans*

For the NL5901 strain in the head region, the analysis of α-syn inclusion counts shows that, when compared to the control group, day 5 did not result in significant differences for any of the experimental groups, Figure 9. However, by day 10, S-PG and S-PS diets significantly decreased α-syn inclusion counts. By day 15, S-PC, S-PG, and S-PS diets all had significantly lower inclusion counts compared to the control. These results suggest that experimental diets influence α-syn

deposition, especially after prolonged exposure, with S-PC, S-PG, and S-PS consistently showing reductions in the number of inclusions.

Further comparisons to day 1 showed significant increases in inclusion counts for the control group at days 10 and 15, suggesting a natural progression of α-syn accumulation over time. For the diet groups, S-CL, S-PC, and U-PC demonstrated higher α-syn inclusion counts on day 10, while no significant changes were observed for the S-PG and S-PS groups across all days. These findings indicate that the inclusion counts are influenced by diet, with S-PC, S-PG, and S-PS showing potential for reducing α-syn accumulation, especially at later time points.

3 | DISCUSSION

The reported results showed that both PC and CL LUVs exerted very little, if any, effect on the rate of α-syn aggregation. These findings are consistent with the previously reported study by Dou and co-workers (Dou et al., 2023; Dou & Kurouski, 2022a) Specifically, it was found that PS LUVs only slightly accelerated the rate of α-syn aggregation. It should be noted that the previously reported results by Dou and co-workers demonstrated that 14-carbon atom long FAs in PC (DMPC) LUVs strongly inhibited α-syn aggregation (Dou et al., 2023; Dou & Kurouski, 2022a). However, 16-carbon atom long PC (DPPC) used in the current study did alter the rate of protein aggregation. These results point to the importance of hydrophobic interactions that take place upon interactions between α-syn and lipids. Thus, the difference in two carbons in FAs of PC results in the drastic changes that the lipid exerts on α-syn aggregation. Previously reported NMR results confirmed that such interactions play an important role in α-syn stability (Giasson et al., 2001; Ueda et al., 1993; Viennet et al., 2018). Specifically, it was found that, in addition to electrostatic interactions that took place between the positively charged amino acid residues of α-syn N-termini and negatively charged heads of lipids, hydrophobic interactions determine the stability of α-syn:lipid complex. NMR results showed that such hydrophobic interactions could be developed between FAs of lipids and aliphatic amino acids of the protein that were primarily located in the NAC domain (Giasson et al., 2001; Ueda et al., 1993; Viennet et al., 2018). Numerous studies reported by the Claessens group indicated that such interactions are directly controlled by the charge and the size of lipid vesicles (Iyer et al., 2014; Iyer & Claessens, 2019; Iyer, Roeters, et al., 2016; Iyer, Schilderink, et al., 2016; Middleton & Rhoades, 2010; Stockl et al., 2008; van Rooijen et al., 2009). At the same time, these protein-lipid interactions, as well as the presence of lipids in the structure of oligomers, as revealed by AFM-IR, indicate that It is possible that there is an undetected kinetic phase that converts secondary structural elements, a process that was previously observed in our group (Zhou & Kurouski, 2020a).

We also found that lipids strongly enhance α-syn oligomer toxicity. Similar effects were also observed by Zhaliazka et al. for the amyloid $\beta_{1\text{-}42}$ peptide (Zhaliazka, Matveyenka, et al., 2023). However, PC and CL had the opposite effects on the toxicity of insulin and lysozyme. Specifically, Matveyenka and co-workers found that these and other phospho- and sphingolipids lowered the toxicity of oligomers and fibrils of insulin and lysozyme (Matveyenka, Rizevsky, & Kurouski, 2022a, 2023; Matveyenka, Rizevsky, Pellois, et al., 2023; Matveyenka, Zhaliazka, et al., 2022; Matveyenka, Zhaliazka, et al., 2023). One can expect that protein-lipid interactions, which would be directly determined by the amino acid sequence of the proteins, could determine an increase or a decrease in the toxicity of amyloid aggregates formed in the presence of lipids.

Our in vitro results also suggest that mitochondrial lipids may play an important role in the onset and spread of PD triggering α-syn aggregation. Both PC and CL constitute a substantial portion of the mitochondrial membrane. One can expect that α-syn interactions with such lipids can yield highly toxic oligomers (Cascella et al., 2021; Chen et al., 2015; Fusco et al., 2017; Zhou & Kurouski, 2020b). Our data indicate that such oligomers cause impairment of mitochondrial activity and enhance ROS production in the cell, which ultimately leads to cell death. It should be noted that there is no clear understanding of whether α-syn aggregation is initiated inside the cell, or whether such oligomers are primarily formed on the outer surface of plasma membranes. Our previous studies showed that in the latter case, protein aggregates formed in the extracellular space can get inside the cell by endocytosis (Matveyenka, Rizevsky, Pellois, et al., 2023). Both oligomers and fibrils then damage endosomes escaping to the cell cytosol, where they enhance ROS levels and damage the endoplasmic reticulum and mitochondria (Matveyenka, Rizevsky, Pellois, et al., 2023; Zhaliazka et al., 2024; Zhaliazka & Kurouski, 2024). A combination of both intra- and extracellular mechanisms of α-syn is likely involved in the onset and spread of PD (Zhaliazka et al., 2024). Nevertheless, protein–lipid interactions that uniquely alter the toxicity of such aggregates should be strongly considered in the design of potential drug candidates that can be used to treat PD. Previously reported results by our group showed that protein aggregates accumulated in cell endosomes (Ali et al., 2025; Matveyenka et al., 2024). This results in severe damage to these organelles and a leakage of protein aggregates into the cytosol, where they trigger a strong ROS response. Leakage of protein aggregates into the cytosol also

allows for their interaction with cell mitochondria, which causes substantial depolarization of mitochondrial membranes, which ultimately leads to cell death.

In this study, we also examined the effects of different phospholipid diets, with varying saturation and polar head groups, on the lifespan, behavior, and α-syn aggregation in *C. elegans*. Both the wild-type N2 strain and the transgenic NL5901 strain, which expresses α-syn fused to YFP in muscle cells, were exposed to diets containing saturated and unsaturated phospholipids, including cardiolipin (CL), phosphatidylcholine (PC), phosphatidylserine (PS), phosphatidylglycerol (PG), and the respective unsaturated and saturated forms.

Our Kaplan–Meier survival curve analyses revealed significant differences in the effects of various phospholipid diets on the lifespan of *C. elegans*. Unsaturated phospholipids, particularly U-PC and U-CL, caused dramatic reductions in lifespan in both N2 and NL5901 strains. The N2 strain had median lifespans of 4 and 15 days when fed U-PC and U-CL, respectively, compared to the control diet's median lifespan of 24 days. Similarly, the NL5901 strain exhibited even more pronounced effects, with median lifespans of 10 days for U-PC and 7 days for U-CL, compared to the control group's lifespan of 25 days. These results underscore the harmful impact of unsaturated phospholipids, which were consistently more detrimental than their saturated counterparts. In contrast, saturated phospholipids, such as S-PC, S-CL, and S-PG, did not significantly affect lifespan, with median values close to those of the control group. These findings suggest that the presence of unsaturated bonds, particularly in the polar head groups, may be a key factor driving the observed toxicity, with the unsaturated diets exacerbating the mortality risk in *C. elegans*, especially in the NL5901 strain.

The Cox proportional hazards model further supported these observations, revealing that unsaturated diets, particularly U-PC and U-CL, were significantly associated with increased mortality risk in both strains. For instance, the hazard ratio for U-PC in the N2 strain was 4.265 ($p < 0.001$), and for NL5901, it was 5.244 ($p < 0.001$), indicating a substantial increase in mortality. Upon using a Wald test, we identified that NL5901 worms were four times more susceptible to mortality on a U-CL diet than wild-type worms. This indicates there may be a greater propensity for U-CL to increase the rate of propagation than other lipid diets. Notably, saturated diets like S-PG and S-PS showed no significant increase in mortality, confirming that these diets do not exacerbate lifespan reduction.

Behavioral assays, specifically swimming assays, highlighted the time-dependent effects of diet on the activity of *C. elegans*. For the N2 strain, swimming activity was significantly reduced by day 5 for worms fed S-CL, S-PS, U-CL, and U-PC diets. By day 10, only worms fed S-PS and U-CL continued to exhibit decreased swimming activity. Interestingly, by day 15, no significant differences were observed in swimming activity across diets. These findings suggest that the unsaturated phospholipids, particularly U-PC, might have a more immediate detrimental effect on swimming behavior, but the effects might not persist over extended periods.

In contrast, the NL5901 strain showed a different pattern of results. The unsaturated diets, particularly U-PC and U-CL, led to sustained reductions in swimming activity over time, with significant decreases observed starting at day 5. This suggests that the transgenic NL5901 strain might be more sensitive to these dietary changes, possibly due to the expression of α-syn and its effects on the worm's neural and muscular functions. Moreover, the persistent reduction in swimming activity observed in the NL5901 strain indicates that the unsaturated diets have a more profound and long-lasting impact on behavior in this strain compared to N2.

In terms of α-syn aggregation, we observed that the dietary composition influenced the accumulation of α-syn inclusions in the head region of NL5901 worms. By day 10, worms fed S-PG and S-PS had significantly fewer α-syn inclusions compared to the control group, suggesting that these diets may have a protective effect against α-syn aggregation. By day 15, S-PC, S-PG, and S-PS were associated with a further reduction in inclusion counts, highlighting the potential of these diets to mitigate the progression of α-syn aggregation over time.

Interestingly, worms fed unsaturated diets, particularly U-PC, showed an increase in α-syn inclusion counts by day 10. However, there was an insufficient number of worms for analysis on days 10 and 15 of the U-CL diet, meaning conclusions cannot be drawn regarding the effects of this lipid on α-syn aggregation. These results suggest that unsaturated diets may exacerbate α-syn aggregation, particularly at earlier time points, which could have implications for neurodegenerative diseases such as PD, where α-syn accumulation is a hallmark.

Overall, the results from our in vivo study provide compelling evidence that phospholipid composition significantly impacts the lifespan, behavior, and α-synuclein aggregation in *C. elegans*. Unsaturated phospholipids, particularly U-PC and U-CL, were found to be more toxic, leading to reduced lifespan, impaired swimming behavior, and increased α-syn inclusions. The transgenic NL5901 strain, which expresses α-syn, appeared to be more sensitive to these dietary changes, emphasizing the role of α-synuclein expression in modulating the effects of phospholipids. These findings suggest that unsaturated phospholipids, by altering membrane dynamics and potentially influencing protein aggregation, may play a crucial role in

neurodegeneration. Further research into the molecular mechanisms behind these effects will be important for understanding the potential link between diet, phospholipid composition, and neurodegenerative diseases in higher organisms.

4 | EXPERIMENTAL METHODS

4.1 | Materials

α-syn was purchased from AnaSpec, CA, USA and used as received; 1,2-dipalmitoyl-sn-glycero-3-phosphocholine (DPPC s-PC), 1,2-dioleoyl-sn-glycero-3-phosphocholine (DOPC, u-PC), 3′-bis[1,2-distearoyl-sn-glycero-3-phospho]-glycerol (s-CL) and 3′-bis[1,2-dilinoleoyl-sn-glycero-3-phospho]-glycerol (u-CL) were purchased from Avanti, AL, USA.

4.2 | LUVs preparation

First, lipid and lipid mixtures were dissolved in chloroform. The mixtures were dried under a fume hood overnight and then re-suspended in 1X PBS buffer. Lipid solutions were vortexed and immersed in an ultrasound bath for 30 s to fully dissolve the lipid. Next, the solutions were placed in a water bath pre-heated to 65°C. After that, the sample was placed into liquid nitrogen with subsequent thawing in a 65°C water bath. The cycle was repeated 5 times, followed by sonication every time before freezing. After 5 cycles, the solutions of lipids were passed through a 100 nm membrane placed into the extruder (Avanti, AL, USA). Dynamic light scattering (DLS) was used to determine the size of the final LUVs.

4.3 | Sample preparation and kinetic measurements

α-syn was dissolved in PBS buffer, pH 7.5 to reach the final concentration of 200 μM. For all protein:lipid samples, the α-syn solution was mixed with LUVs at a 1:2 protein:lipid ratio with the final concentration of α-syn of 100 μM. Samples were incubated at 37°C under 510 RPM shaking at pH 7.4 in the plate reader (Tecan, Männedorf, Switzerland). α-syn aggregation was monitored using thioflavin T (ThT) fluorescence assay. ThT was added to the samples to reach the final concentration of ThT of 25 μM. Samples were incubated at 37°C under 510 RPM shaking at pH 7.4 in the plate reader (Tecan, Männedorf, Switzerland). Excitation was 450 nm; the emission signal was collected at 490 nm. Each measurement was done in triplicate.

4.4 | AFM-IR imaging and spectroscopy

The solution (3–6 μL) of protein aggregate samples was deposited onto a silicon wafer and exposed to it for 5–10 min. Next, the excess of the sample was removed; the sample surface was rinsed with DI water and dried under nitrogen flow. AFM-IR imaging was conducted using a Nano-IR3 system (Bruker, Santa Barbara, CA, USA). The IR source was a QCL laser. Contact-mode AFM tips (ContGB-G AFM probe, NanoAndMore) were used to obtain all spectra and maps. No evidence of sample distortion was observed upon contact-mode AFM imaging. IR maps at 1624, 1655, and 1694 cm^{-1} wavenumber values were obtained to study the secondary structure of α-syn:PS and α-syn:PC oligomers. Phase loop lock was enabled during the mapping with a 0.03 V threshold. iGain and pGain varied based on different particle heights, but in general from 0.5 to 1 for iGain and 1 to 2 for pGain. The scan rate is 0.6 Hz and resolution X and Y is 256 pts. AFM height and deflection images were acquired simultaneously with IR maps. Twenty-point measurements were taken from every analyzed oligomer and individual aggregates. The spectra were zapped from 1648 to 1652 cm^{-1} due to chip-to-chip transition artifacts from the instrument. The spectra resolution is 2 cm^{-1}/pt. Savitzky–Golay smoothing was applied to all spectra with 2 polynomial orders by using MATLAB.

4.5 | Cell toxicity assay

Rat midbrain N27 cells, a model cell line for PD, grew in RPMI 1640 Medium (Thermo Fisher Scientific, Waltham, MA, USA) with 10% fetal bovine serum (FBS) (Invitrogen, Waltham, MA, USA) in a 96 well-plate (5000 cells per well) at 37°C under 5% CO_2. After 24 h, the cells were found to fully adhere to the wells, reaching ∼70% confluency. Next, 100 μL of the cell culture was replaced with 100 μL RPMI 1640 Medium with 5% FBS-containing protein samples. After 48 h of incubation with the protein aggregates, a lactate dehydrogenase (LDH) assay was performed on the cell medium using the CytoTox 96 non-radioactive cytotoxicity assay (G1781, Promega, Madison, WI, USA). Absorption measurements were made in a plate reader (Tecan, Männedorf, Switzerland) at 490 nm. All experiments were done in triplicates. Every well was measured 25 times in different locations. In parallel, a reactive oxygen species (ROS) assay was performed using the same cell culture. Briefly, ROS reagent (C10422, Invitrogen, Waltham, MA, USA) was added to reach the final concentration of 5 μM and incubated at 37°C under 5% CO_2 for 30 min. After the supernatant was removed, the cells were washed with PBS and resuspended in 200 μL of PBS in the flow cytometry

tubes. Sample measurements were made in Accuri C6 Flow Cytometer (BD, San Jose, CA, USA) using a red channel ($\lambda = 633$ nm). Percentages of ROS cells were determined using Acura software.

For JC-1 staining, 1 μL of JC-1 reagent (M34152A, Invitrogen) was added to cells and incubated at 37°C under 5% CO_2 for 30 min. After the supernatant was removed, cells were washed with PBS and resuspended in 200 μL of PBS in the flow cytometry tubes. Sample measurements were made in Accuri C6 Flow Cytometer (BD, San Jose, CA, USA) using a red channel ($k = 633$ nm). Percentages of ROS cells were determined using ACCURI software. For both LDH and ROS controls, (PBS) pH 7.4 was added to cells and incubated under the same experimental conditions. *t*-test was used to analyze the results: $*p \leq 0.05$; $**p \leq 0.01$; $***p \leq 0.001$, relative to untreated cells are shown. NS indicates 'non-significant' differences between the toxicity or ROS response of the samples.

4.6 | Utilization of *C. elegans*

C. elegans strain NL5901 was purchased from the University of Minnesota worm bank, and N2 wildtype worms were a kind gift from Dr. Michael Polymenis, Professor at Texas A&M University. Worms were maintained at 20°C on NGM plates seeded with OP50 *E. coli* and allowed to reach an egg-producing age before age synchronizing as previously described (Porta-de-la-Riva et al., 2012). Lipid supplementation was performed by centrifuging concentrated stocks of OP50 *E. coli* for 10 min at 500 rcf, removing half of the supernatant and mixing the remaining with the same volume of suspended phospholipids (in water) to bring the final concentration of phospholipids to 2% (w/v) or 0.02 g/mL. Quickly, 100 μL of these mixtures were pipetted onto 3.5 cm petri dishes and dried and UV-killed for 30 min within a biosafety cabinet. After age synchronization, 3 days were allotted for worms to be at adults, and day 1 adults were then transferred to their respective plates. Each diet started with 100 adult worms spread over 10 Petri dishes each 3.5 cm in diameter with NGM and *E. coli* or NGM and lipid-supplemented *E. coli* per diet (10 worms on plate). Throughout the experiment, worms were kept at 20°C.

4.7 | Lifespan assay

Lifespan assays were performed by recording the number of live and dead worms daily. These data were used to calculate daily survival probabilities during adulthood using the Kaplan–Meier estimator. Kaplan–Meier survival curves were generated with the RStudio libraries "survival" and "survminer." Confidence intervals for the survival probabilities were estimated using Greenwood's formula for variance and a log-transformation to ensure valid bounds. To assess the effect of diets on lifespan, a Cox proportional hazards model was applied as a semi-parametric approach for generating hazard ratios. The model and the Wald test were conducted in RStudio using the "survival" library as well.

4.8 | Swimming assay

Swimming assays were performed by counting the number of thrashes per minute. A thrash was defined as a movement where the worm bent its head to one side and then returned to the midline. For each assay, a single worm was placed in a 4 μL droplet of M9 buffer on a glass slide and video-recorded for analysis by multiple observers. The thrash counts were averaged and are reported here. N2 worms used in these assays were discarded after testing, while NL5901 worms were quickly analyzed using fluorescence microscopy and then discarded to avoid influencing the growth or lifespan outcomes of the remaining worms. Statistical comparisons between groups were conducted using the Kruskal–Wallis test followed by Dunn's post hoc test in RStudio, utilizing the "dunn.test" library.

4.9 | Fluorescence microscopy of *C. elegans*

Fluorescence microscopy was performed using an EVOS M5000 imaging system to visualize α-synuclein deposits in NL5901 *C. elegans* over time and under various dietary conditions. These worms express α-synuclein fused to a YFP tag, enabling fluorescence-based observation. To immobilize the worms, a 2 μL droplet of M9 buffer containing 50 mM sodium azide was placed on a glass slide. Using a 20× objective, the head region—defined as the area from the anterior nose to the posterior pharynx—was imaged under GFP emission settings. Bright circular inclusions were counted by multiple researchers, and the results were averaged and reported here. Statistical comparisons between groups were conducted using the Kruskal–Wallis test followed by Dunn's post hoc test with the "dunn.test" library in RStudio.

AUTHOR CONTRIBUTIONS

Aidan P. Holman: Conceptualization; investigation; writing – original draft; methodology; visualization; writing – review and editing; validation. **Tianyi Dou:** Conceptualization; investigation; writing – original draft; methodology; validation; visualization; writing – review and editing. **Mikhail Matveyenka:** Investigation; methodology; validation; writing – review and editing. **Kiryl Zhaliazka:** Investigation; writing – review and editing.

Anjni Patel: Investigation. **Avery Maalouf:** Investigation. **Ragd Elsaigh:** Investigation. **Dmitry Kurouski:** Conceptualization; funding acquisition; writing – original draft; writing – review and editing; project administration; supervision; resources.

ACKNOWLEDGMENTS

We would like to thank Cole Sebok for his help with the in vivo assay. We are grateful to the National Institutes of Health for the provided financial support (R35GM142869).

CONFLICT OF INTEREST STATEMENT

The authors declare no conflict of interests.

DATA AVAILABILITY STATEMENT

The data that support the findings of this study are available from the corresponding author upon reasonable request.

ORCID

Dmitry Kurouski https://orcid.org/0000-0002-6040-4213

REFERENCES

Ali A, Matveyenka M, Pickett DN, Rodriguez A, Kurouski D. Tubulin-binding region modulates cholesterol-triggered aggregation of tau proteins. J Neurochem. 2025;169:e16294.

Banerjee S, Ghosh A. Structurally distinct polymorphs of tau aggregates revealed by nanoscale infrared spectroscopy. J Phys Chem Lett. 2021;12:11035–41.

Cascella R, Chen SW, Bigi A, Camino JD, Xu CK, Dobson CM, et al. The release of toxic oligomers from α-synuclein fibrils induces dysfunction in neuronal cells. Nat Commun. 2021;12:1814.

Centrone A. Infrared imaging and spectroscopy beyond the diffraction limit. Annu Rev Anal Chem. 2015;8:101–26.

Chae J, Dong Q, Huang J, Centrone A. Chloride incorporation process in CH(3)NH(3)PbI(3-x)Cl(x) perovskites via nanoscale bandgap maps. Nano Lett. 2015;15:8114–21.

Chen SW, Drakulic S, Deas E, Ouberai M, Aprile FA, Arranz R, et al. Structural characterization of toxic oligomers that are kinetically trapped during alpha-synuclein fibril formation. Proc Natl Acad Sci U S A. 2015;112:E1994–2003.

Chiti F, Dobson CM. Protein misfolding, amyloid formation, and human disease: a summary of progress over the last decade. Annu Rev Biochem. 2017;86:27–68.

Choi J, Yin T, Shinozaki K, Lampe JW, Stevens JF, Becker LB, et al. Comprehensive analysis of phospholipids in the brain, heart, kidney, and liver: brain phospholipids are least enriched with polyunsaturated fatty acids. Mol Cell Biochem. 2018;442:187–201.

Cremades N, Cohen SI, Deas E, Abramov AY, Chen AY, Orte A, et al. Direct observation of the interconversion of normal and toxic forms of alpha-synuclein. Cell. 2012;149:1048–59.

Dazzi A, Prater CB. AFM-IR: technology and applications in nanoscale infrared spectroscopy and chemical imaging. Chem Rev. 2017;117:5146–73.

Dazzi A, Prater CB, Hu QC, Chase DB, Rabolt JF, Marcott C. AFM-IR: combining atomic force microscopy and infrared spectroscopy for nanoscale chemical characterization. Appl Spectrosc. 2012;66:1365–84.

Dou T, Kurouski D. Phosphatidylcholine and phosphatidylserine uniquely modify the secondary structure of alpha-Synuclein oligomers formed in their presence at the early stages of protein aggregation. ACS Chem Neurosci. 2022a;13:2380–5.

Dou T, Kurouski D. Phosphatidylcholine and phosphatidylserine uniquely modify the secondary structure of α-synuclein oligomers formed in their presence at the early stages of protein aggregation. ACS Chem Neurosci. 2022b;13(16):2380–5. https://doi.org/10.1021/acschemneuro.2c00355

Dou T, Li Z, Zhang J, Evilevitch A, Kurouski D. Nanoscale structural characterization of individual viral particles using atomic force microscopy infrared spectroscopy (AFM-IR) and tip-enhanced Raman spectroscopy (TERS). Anal Chem. 2020;92:11297–304.

Dou T, Matveyenka M, Kurouski D. Elucidation of secondary structure and toxicity of alpha-synuclein oligomers and fibrils grown in the presence of phosphatidylcholine and phosphatidylserine. ACS Chem Neurosci. 2023;14:3183–91.

Dou T, Zens C, Schröder K, Jiang Y, Makarov AA, Kupfer S, et al. Solid-to-liposome conformational transition of phosphatidylcholine and phosphatidylserine probed by atomic force microscopy, infrared spectroscopy, and density functional theory calculations. Anal Chem. 2022;94:13243–9.

Dou T, Zhou L, Kurouski D. Unravelling the structural organization of individual α-synuclein oligomers grown in the presence of phospholipids. J Phys Chem Lett. 2021;12:4407–14.

Dudek J. Role of cardiolipin in mitochondrial signaling pathways. Frontiers Cell Dev Biol. 2017;5:90.

Frese A, Goode C, Zhaliazka K, Holman AP, Dou T, Kurouski D. Length and saturation of fatty acids in phosphatidylserine determine the rate of lysozyme aggregation simultaneously altering the structure and toxicity of amyloid oligomers and fibrils. Protein Sci. 2023;32:e4717.

Frieg B, Antonschmidt L, Dienemann C, Geraets JA, Najbauer EE, Matthes D, et al. The 3D structure of lipidic fibrils of alpha-synuclein. Nat Commun. 2022;13:6810.

Fusco G, Chen SW, Williamson PTF, Cascella R, Perni M, Jarvis JA, et al. Structural basis of membrane disruption and cellular toxicity by α-synuclein oligomers. Science. 2017;358:1440–3.

Galvagnion C. The role of lipids interacting with α-synuclein in the pathogenesis of Parkinson's disease. J Parkinsons Dis. 2017;7:433–50.

Galvagnion C, Brown JW, Ouberai MM, Flagmeier P, Vendruscolo M, Buell AK, et al. Chemical properties of lipids strongly affect the kinetics of the membrane-induced aggregation of alpha-synuclein. Proc Natl Acad Sci USA. 2016;113:7065–70.

Galvagnion C, Buell AK, Meisl G, Michaels TC, Vendruscolo M, Knowles TP, et al. Lipid vesicles trigger alpha-synuclein aggregation by stimulating primary nucleation. Nat Chem Biol. 2015a;11:229–34.

Galvagnion C, Buell AK, Meisl G, Michaels TCT, Vendruscolo M, Knowles TPJ, et al. Lipid vesicles trigger α-synuclein aggregation by stimulating primary nucleation. Nat Chem Biol. 2015b;11:229–34.

Giasson BI, Murray IV, Trojanowski JQ, Lee VM. A hydrophobic stretch of 12 amino acid residues in the middle of alpha-synuclein is essential for filament assembly. J Biol Chem. 2001;276:2380–6.

Guerrero-Ferreira R, Kovacik L, Ni D, Stahlberg H. New insights on the structure of alpha-synuclein fibrils using cryo-electron microscopy. Curr Opin Neurobiol. 2020;61:89–95.

Guerrero-Ferreira R, Taylor NM, Mona D, Ringler P, Lauer ME, Riek R, et al. Cryo-EM structure of alpha-synuclein fibrils. eLife. 2018;7:e36402.

Heise H, Hoyer W, Becker S, Andronesi OC, Riedel D, Baldus M. Molecular-level secondary structure, polymorphism, and dynamics of full-length alpha-synuclein fibrils studied by solid-state NMR. Proc Natl Acad Sci U S A. 2005;102:15871–6.

Iyer A, Claessens M. Disruptive membrane interactions of alpha-synuclein aggregates. Biochim Biophys Acta Proteins Proteom. 2019;1867:468–82.

Iyer A, Petersen NO, Claessens MM, Subramaniam V. Amyloids of alpha-synuclein affect the structure and dynamics of supported lipid bilayers. Biophys J. 2014;106:2585–94.
Iyer A, Roeters SJ, Schilderink N, Hommersom B, Heeren RM, Woutersen S, et al. The impact of N-terminal acetylation of alpha-synuclein on phospholipid membrane binding and fibril structure. J Biol Chem. 2016;291:21110–22.
Iyer A, Schilderink N, Claessens M, Subramaniam V. Membrane-bound alpha synuclein clusters induce impaired lipid diffusion and increased lipid packing. Biophys J. 2016;111:2440–9.
Jiang Z, de Messieres M, Lee JC. Membrane remodeling by alpha-synuclein and effects on amyloid formation. J Am Chem Soc. 2013;135:15970–3.
Katzenmeyer AM, Chae J, Kasica R, Holland G, Lahiri B, Centrone A. Nanoscale imaging and spectroscopy of plasmonic modes with the PTIR technique. Adv Opt Mater. 2014;2:718–22.
Kotarek JA, Moss MA. Impact of phospholipid bilayer saturation on amyloid-β protein aggregation intermediate growth: a quartz crystal microbalance analysis. Anal Biochem. 2010;399:30–8.
Kurouski D, Dazzi A, Zenobi R, Centrone A. Infrared and Raman chemical imaging and spectroscopy at the nanoscale. Chem Soc Rev. 2020;49:3315–47.
Li B, Ge P, Murray KA, Sheth P, Zhang M, Nair G, et al. Cryo-EM of full-length α-synuclein reveals fibril polymorphs with a common structural kernel. Nat Commun. 2018;9(1):3609. https://doi.org/10.1038/s41467-018-05971-2
Matveyenka M, Rizevsky S, Kurouski D. The degree of unsaturation of fatty acids in phosphatidylserine alters the rate of insulin aggregation and the structure and toxicity of amyloid aggregates. FEBS Lett. 2022a;596:1424–33.
Matveyenka M, Rizevsky S, Kurouski D. Length and unsaturation of fatty acids of phosphatidic acid determines the aggregation rate of insulin and modifies the structure and toxicity of insulin aggregates. ACS Chem Neurosci. 2022b;13:2483–9.
Matveyenka M, Rizevsky S, Kurouski D. Unsaturation in the fatty acids of phospholipids drastically alters the structure and toxicity of insulin aggregates grown in their presence. J Phys Chem Lett. 2022c;13:4563–9.
Matveyenka M, Rizevsky S, Kurouski D. Elucidation of the effect of phospholipid charge on the rate of insulin aggregation and structure and toxicity of amyloid fibrils. ACS Omega. 2023;8:12379–86.
Matveyenka M, Rizevsky S, Pellois JP, Kurouski D. Lipids uniquely alter rates of insulin aggregation and lower toxicity of amyloid aggregates. Biochim Biophys Acta Mol Cell Biol Lipids. 2023;1868:159247.
Matveyenka M, Zhaliazka K, Kurouski D. Unsaturated fatty acids uniquely alter aggregation rate of α-synuclein and insulin and change the secondary structure and toxicity of amyloid aggregates formed in their presence. FASEB J. 2023;37(7):e22972. https://doi.org/10.1096/fj.202300003R
Matveyenka M, Zhaliazka K, Kurouski D. Macrophages and natural killers degrade alpha-synuclein aggregates. Mol Pharm. 2024;21:2565–76.
Matveyenka M, Zhaliazka K, Rizevsky S, Kurouski D. Lipids uniquely alter secondary structure and toxicity of lysozyme aggregates. FASEB J. 2022;36:e22543.
Middleton ER, Rhoades E. Effects of curvature and composition on alpha-synuclein binding to lipid vesicles. Biophys J. 2010;99:2279–88.
O'Leary EI, Lee JC. Interplay between alpha-synuclein amyloid formation and membrane structure. Biochim Biophys Acta Proteins Proteom. 2019a;1867:483–91.
O'Leary EI, Lee JC. Interplay between α-synuclein amyloid formation and membrane structure. Biochim Biophys Acta (BBA) Proteins Proteomics. 2019b;1867:483–91.
Paradies G, Paradies V, Ruggiero FM, Petrosillo G. Role of cardiolipin in mitochondrial function and dynamics in health and disease: molecular and pharmacological aspects. Cells. 2019;8:728.
Pfefferkorn CM, Jiang Z, Lee JC. Biophysics of alpha-synuclein membrane interactions. Biochim Biophys Acta. 2012;1818:162–71.
Pirc K, Ulrih NP. A-synuclein interactions with phospholipid model membranes: key roles for electrostatic interactions and lipid-bilayer structure. Biochim Biophys Acta (BBA) Biomemb. 2015;1848:2002–12.
Poewe W, Seppi K, Tanner CM, Halliday GM, Brundin P, Volkmann J, et al. Parkinson disease. Nat Rev Dis Primers. 2017;3:17013.
Porta-de-la-Riva M, Fontrodona L, Villanueva A, Cerón J. Basic Caenorhabditis elegans methods: synchronization and observation. J Vis Exp. 2012;64:e4019.
Rambaran RN, Serpell LC. Amyloid fibrils: abnormal protein assembly. Prion. 2008;2:112–7.
Ramer G, Aksyuk VA, Centrone A. Quantitative chemical analysis at the nanoscale using the photothermal induced resonance technique. Anal Chem. 2017;89:13524–31.
Ramer G, Ruggeri FS, Levin A, Knowles TPJ, Centrone A. Determination of polypeptide conformation with nanoscale resolution in water. ACS Nano. 2018;12:6612–9.
Ruggeri FS, Benedetti F, Knowles TPJ, Lashuel HA, Sekatskii S, Dietler G. Identification and nanomechanical characterization of the fundamental single-strand protofilaments of amyloid alpha-synuclein fibrils. Proc Natl Acad Sci USA. 2018;115:7230–5.
Ruggeri FS, Charmet J, Kartanas T, Peter Q, Chia S, Habchi J, et al. Microfluidic deposition for resolving single-molecule protein architecture and heterogeneity. Nat Commun. 2018;9:3890.
Ruggeri FS, Flagmeier P, Kumita JR, Meisl G, Chirgadze DY, Bongiovanni MN, et al. The influence of pathogenic mutations in α-synuclein on biophysical and structural characteristics of amyloid fibrils. ACS Nano. 2020;14:5213–22.
Ruggeri FS, Longo G, Faggiano S, Lipiec E, Pastore A, Dietler G. Infrared nanospectroscopy characterization of oligomeric and fibrillar aggregates during amyloid formation. Nat Commun. 2015;6:7831.
Sidhu A, Wersinger C, Vernier P. Alpha-synuclein regulation of the dopaminergic transporter: a possible role in the pathogenesis of Parkinson's disease. FEBS Lett. 2004;565:1–5.
Stockl M, Fischer P, Wanker E, Herrmann A. Alpha-synuclein selectively binds to anionic phospholipids embedded in liquid-disordered domains. J Mol Biol. 2008;375:1394–404.
Trostchansky A, Lind S, Hodara R, Oe T, Blair IA, Ischiropoulos H, et al. Interaction with phospholipids modulates α-synuclein nitration and lipid–protein adduct formation. Biochem J. 2005;393:343–9.
Tuttle MD, Comellas G, Nieuwkoop AJ, Covell DJ, Berthold DA, Kloepper KD, et al. Solid-state NMR structure of a pathogenic fibril of full-length human α-synuclein. Nat Struct Mol Biol. 2016;23:409–15.
Ueda K, Fukushima H, Masliah E, Xia Y, Iwai A, Yoshimoto M, et al. Molecular cloning of cDNA encoding an unrecognized component of amyloid in Alzheimer disease. Proc Natl Acad Sci U S A. 1993;90:11282–6.
van Rooijen BD, Claessens MM, Subramaniam V. Lipid bilayer disruption by oligomeric alpha-synuclein depends on bilayer charge and accessibility of the hydrophobic core. Biochim Biophys Acta. 2009;1788:1271–8.
Viennet T, Wordehoff MM, Uluca B, Poojari C, Shaykhalishahi H, Willbold D, et al. Structural insights from lipid-bilayer nanodiscs link alpha-synuclein membrane-binding modes to amyloid fibril formation. Commun Biol. 2018;1:44.
Wischik CM, Crowther RA, Stewart M, Roth M. Subunit structure of paired helical filaments in Alzheimer's disease. J Cell Biol. 1985;100:1905–12.
Wischik CM, Novak M, Thogersen HC, Edwards PC, Runswick MJ, Jakes R, et al. Isolation of a fragment of tau derived from the

core of the paired helical filament of Alzheimer disease. Proc Natl Acad Sci U S A. 1988;85:4506–10.
Yamada K, Iwatsubo T. Extracellular α-synuclein levels are regulated by neuronal activity. Mol Neurodegener. 2018;13:9.
Zhaliazka K, Ali A, Kurouski D. Phospholipids and cholesterol determine molecular mechanisms of cytotoxicity of alpha-synuclein oligomers and fibrils. ACS Chem Neurosci. 2024; 15:371–81.
Zhaliazka K, Kurouski D. Nanoscale characterization of parallel and antiparallel beta-sheet amyloid beta 1-42 aggregates. ACS Chem Neurosci. 2022;13:2813–20.
Zhaliazka K, Kurouski D. Nano-infrared analysis of amyloid beta(1–42) fibrils formed in the presence of lipids with unsaturated fatty acids. Nanoscale. 2023;15:19650–7.
Zhaliazka K, Kurouski D. Elucidation of molecular mechanisms by which amyloid beta (1) (−) (42) fibrils exert cell toxicity. Biochim Biophys Acta Mol Cell Biol Lipids. 2024;1869:159510.
Zhaliazka K, Matveyenka M, Kurouski D. Lipids uniquely alter the secondary structure and toxicity of amyloid beta 1–42 aggregates. FEBS J. 2023;290:3203–20. https://doi.org/10.1111/febs.16738
Zhaliazka K, Serada V, Matveyenka M, Rizevsky S, Kurouski D. Protein-to-lipid ratio uniquely changes the rate of lysozyme aggregation but does not significantly alter toxicity of mature protein aggregates. Biochim Biophys Acta Mol Cell Biol Lipids. 2023; 1868:159305.
Zhou L, Kurouski D. Structural characterization of individual alpha-synuclein oligomers formed at different stages of protein aggregation by atomic force microscopy-infrared spectroscopy. Anal Chem. 2020a;92:6806–10.
Zhou L, Kurouski D. Structural characterization of individual α-synuclein oligomers formed at different stages of protein aggregation by atomic force microscopy-infrared spectroscopy. Anal Chem. 2020b;92:6806–10.

SUPPORTING INFORMATION

Additional supporting information can be found online in the Supporting Information section at the end of this article.

How to cite this article: Holman AP, Dou T, Matveyenka M, Zhaliazka K, Patel A, Maalouf A, et al. The role of phospholipid saturation and composition in α-synuclein aggregation and toxicity: A dual in vitro and in vivo approach. Protein Science. 2025;34(5):e70121. https://doi.org/10.1002/pro.70121